

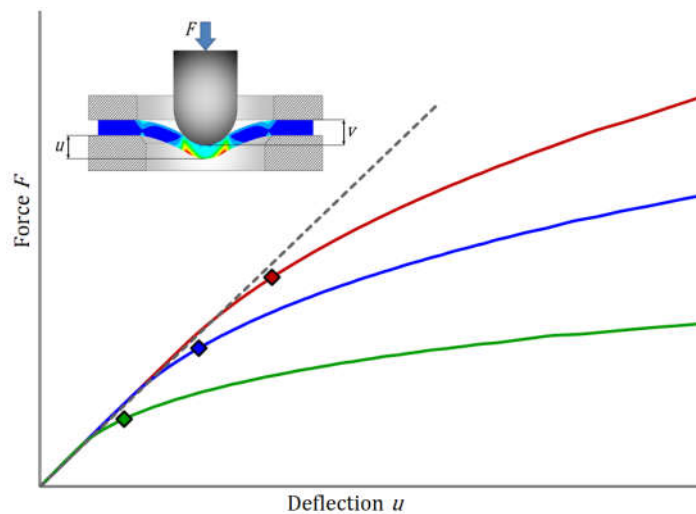
An improved correlation for the estimation of the yield strength from small punch testing

Eberhard Altstadt

Helmholtz-Zentrum Dresden-Rossendorf, Bautzner Landstrasse 400, 01328 Dresden, Germany

* Correspondence: e.altstadt@hzdr.de

Abstract: This study aims at improving the empirical correlation for estimating the yield strength from small punch tests. The currently used procedure in the European standard EN 10371 to determine the elastic-plastic transition force – based on bi-linear fitting – involves a dependency not only on the onset of plastic flow but also on the work hardening of the material. Consequently, the yield strength correlation factor is not universal but depends on the material properties and on the geometry of the small punch set-up – leading to a significant uncertainty in the yield strength estimation. In this study, an alternative definition of the elastic-plastic transition force is proposed, which significantly less depends on the work hardening of the material and on the small punch geometry. The approach is based on extensive elastic-plastic finite element simulations with generic material properties, including a systematic variation of the yield strength, ultimate tensile strength, and uniform elongation. The new definition of the transition force is based on the deviation of the force-deflection curve from the analytical elastic slope derived by Reissner's plate theory. A significant reduction of the uncertainty of the yield strength estimation is demonstrated.



Citation: To be added by editorial staff during production.

Academic Editor: Firstname Last-name

Received: 16 September 2023

Revised: date

Accepted: date

Published: date



Copyright: © 2023 by the authors.

Submitted for possible open access publication under the terms and conditions of the Creative Commons Attribution (CC BY) license (<https://creativecommons.org/licenses/by/4.0/>).

Keywords: Small punch test; yield strength; empirical correlation; finite element simulation; plate theory

1. Introduction

The small punch (SP), see Figure 2a, test has been established as a small specimen test technology supporting development and screening of structural materials, see e.g. [1–3]. It provides estimations of mechanical properties with small amounts of material and received much attraction as high throughput characterization method. For example, this

is of major interest for irradiated and activated materials [4,5]. The primary output of the quasi-static SP test is the punch force as function of the punch displacement – force-displacement curve $F(v)$ – or as function of specimen deflection – force-deflection curve $F(u)$. A comprehensive discussion on the stages and properties of the force-deflection curve is provided in [3]. In case of SP creep tests, the punch force is kept constant and the displacement and/or deflection is measured as function of time. Recently a European standard has been published [6]. So far, the SP test has been successfully used to estimate (i) the ductile-to-brittle transition temperature where SP tests at different temperatures are used to derive the SP energy as function of test temperature [1,2,7], (ii) tensile properties – in particular the yield strength (YS) and ultimate tensile strength (UTS) [8–12], (iii) fracture and damage parameters [3,13,14] and (iv) creep properties [15–21]. In the European standard [6], the associated methods are described in informative, non-mandatory annexes. The current study is related to (ii), in particular to the estimation of the yield strength from the quasi-static force-deflection curve $F(u)$. Recent developments are focused on the involvement of machine learning [22,23].

The following correlation was proposed for the YS [24]:

$$R_{p02} = \beta_{YS} \cdot F_e/h^2 \quad (1)$$

with h being the initial specimen thickness, F_e the elastic-plastic transition force and β_{YS} an empirical factor. The transition force is determined by a bi-linear fit [6], see Figure 1. Kameda and Mao [24] found $\beta_{YS} = 0.36$ for specimen thicknesses of 0.25 mm and 0.5 mm irrespective of the geometrical parameters of the SPT set-up. In contrast, the European standard suggests a value of $\beta_{YS} = 0.52$. The application and detailed analysis of these empirical correlations shows that the correlation factor for the yield stress depends on the geometrical parameters of the SP test (punch diameter, die diameter, size of die edge radius or chamfer, specimen thickness) and on the material properties.

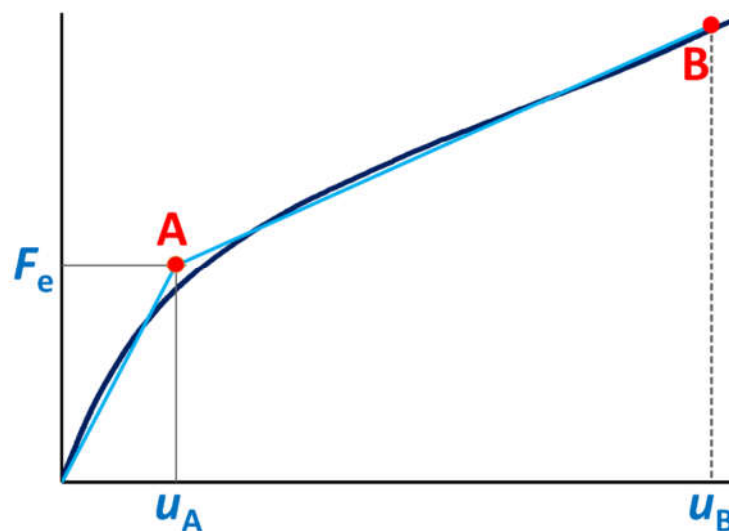


Figure 1. Bi-linear fit to obtain the transition force F_e . The graph represents the early stage of the SP test ($u \leq h$).

In [25] it was demonstrated that the maximum plastic strain in the sample is already around 0.1 when the transition force F_e is reached. Therefore, F_e is not only a function of the flow stress but is also significantly affected by the work hardening of the material (i. e. the slope of the stress-strain curve). Hähner et al. [26] addressed this problem by means of a self-consistent data reduction scheme for the determination of σ_y which was based on the curvature K of the force–displacement curve rather than a single F_e force level. The curvature was estimated from the offset forces at displacement offsets of 10, 50 and 90 μm . Based on systematic FE simulations with a Holomon hardening law ($\sigma = C \cdot \varepsilon^n$) they could relate the hardening exponent n to the curvature K of the force-displacement curve

(C is a material constant). This relation facilitated the establishment of the correlation factor β_{YS} as a function of n , which led to a significant reduction of the uncertainty for the yield strength estimation. In this approach, the correlation factor β_{YS} is material dependent through its dependence on the hardening exponent n .

Another method was proposed by Calaf Chica et al. [9]. Based on FE simulations and experimental SP results, they derived an exponential expression for the yield stress as function of the slope at the first inflection point of the force displacement curve. It was shown that the uncertainty for the yield strength estimation could be reduced as compared to the methods based on equation (1). Nevertheless, the very accurate determination of the slope at the first inflection point is crucial because of the exponential nature of the correlation. In view of measurement accuracy and the compliance of the test set-up, this required accuracy could be problematic in practice.

Yet another method was proposed by Zhong et al. [27]. It is based on extracting true stress–strain curves from SP test data using iterative finite element simulations. The extracted true stress–strain curves were used in FE simulation of tensile tests to obtain the tensile parameters. In this way, a database was created to predict tensile parameters from SP force-deflection curves by means of data mining. The above-mentioned findings in [9,25–27] demonstrate, that the current procedure for the yield strength estimation as established in the standard [6] exhibits a large uncertainty. The motivation of the current work is to identify a possibility for an improvement of the reliability of the YS estimation, while keeping the procedure as simple as possible for the practical application. Therefore, the study still relies on the simple correlation equation (1) – but proposes an alternative definition of the elastic-plastic transition force, which is significantly less dependent on the work hardening of the material. The approach is based on the deviation of the force-deflection curve $F(u)$ from the analytical elastic slope derived by Reissner's plate theory. Moreover, it will be shown that the new definition of the transition force leads to significantly reduced dependence of the correlation factor β_{YS} on the geometry of the SP set-up.

2. Modelling of the small punch test

2.1. Finite element modelling

The basic geometry of a SP set-up is shown in Figure 2. The geometrical parameters are listed in Table 1. For $h = 0.5$ mm, this parameter set represents the default geometry according to the EN standard [6].

Table 1. Geometry parameters of the analyzed SPT set-ups.

Punch diameter $d = 2r$ (mm)	Receiving hole diameter D (mm)	Specimen thickness h (mm)	Edge size (mm)	Edge type
2.5	4.0	0.2 ... 0.6	0.2	Chamfer

The finite element simulations were done with an axisymmetric model including contact and friction. The commercial code ANSYS® 2021.R1 was used. Axisymmetric elements with 8 nodes, elastic-plastic material and large deformation and finite strain capability were used for the SP specimen. The element size was 10 μm . The lower die, the punch and the downholder were modelled by means of rigid lines interacting with the contact elements attached to the specimen surface. In [11], it was shown that the assumption of rigid punch and die has no significant effect on $F(u)$ as compared to an elastic model of punch and die. The friction coefficient for the contact areas between disc and punch was $\mu = 0.2$. The SP disc was fully clamped, i.e., relative motion between SP disc and lower die was prevented.

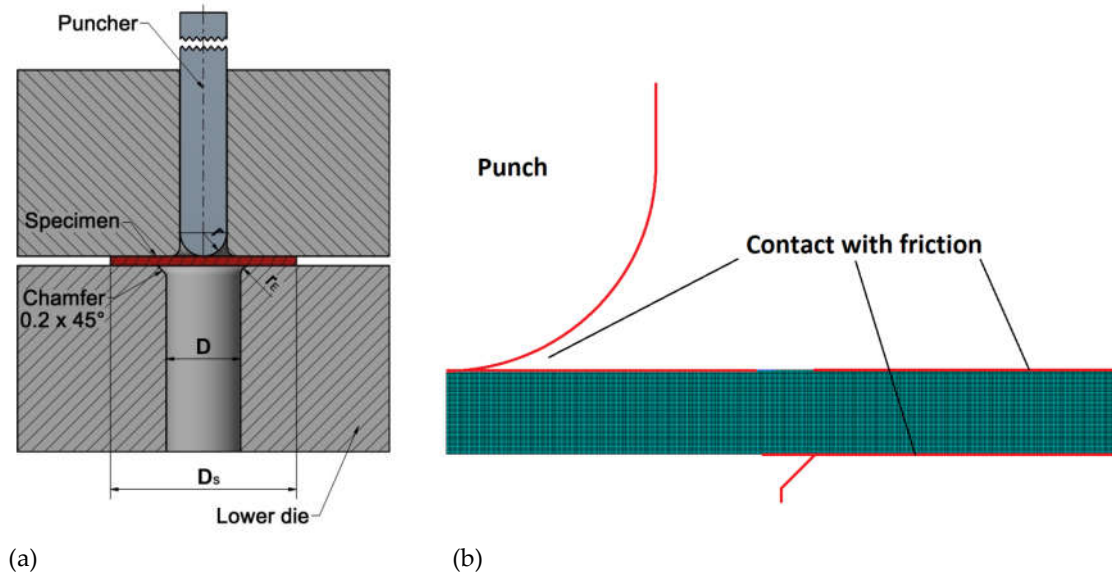


Figure 2. (a) Scheme of a SP test setup the edge of the receiving hole can either be a chamfer or a radius; (b) FE mesh (right).

The plastic deformation was based on the following constitutive equation:

$$\sigma_y(\varepsilon^{pl}) = \sigma_{y0} + r_1 \cdot [\alpha \cdot \varepsilon^{pl} + 1 - \exp(-n\varepsilon^{pl})] \quad (2)$$

where σ is the true equivalent stress and ε^{pl} the true plastic equivalent strain. σ_{y0} , r_1 , α and n are material parameters. The parameter α represents the ratio of linear and exponential hardening. In this study $\alpha = 1$ was chosen. The corresponding uniaxial engineering (nominal) stress-strain curve $\bar{\sigma}(\bar{\varepsilon})$ is obtained by:

$$\bar{\varepsilon}^{to} = \exp[\varepsilon^{pl} + \varepsilon^{el}] - 1 = \exp\left[\varepsilon^{pl} + \frac{\sigma}{E}\right] - 1 \quad (3)$$

$$\bar{\sigma} = \sigma / (1 + \bar{\varepsilon})$$

with E being the elasticity modulus. The overbar indicates engineering (nominal) values. An in-house fitting algorithm was used to determine σ_{y0} , r_1 and n from given values of $R_{p0.2}$, R_m and A_{gt} . The specimen plate is loaded by a stepwise increasing displacement of the punch, v , up to a final value of 1 mm. For the purpose of this investigation, larger displacements are not needed. Consequently, the constitutive equations do not include ductile damage as this develops only at higher displacements [5]. In the postprocessing, two types of SP curves are generated: the force-displacement curve $F(v)$ (reaction force at the pilot node of the punch versus punch displacement) and the force-deflection curve $F(u)$ (reaction force at the pilot node of the punch versus the central bottom deflection of the plate). The difference between v and u equals to the thickness reduction of the disc at the center.

2.2. Analytical equations for the linear elastic phase of the SP test

The analytical description of plate bending is useful for the for determination of the initial slope of the load-deflection curve of a SP test. Figure 3 shows the relevant parameters of a fully clamped circular plate: a - plate radius ($D/2 + r_E$), p_0 - contact pressure between punch and SP specimen, b - radius of the contact area. The contact pressure is simplifying assumed to be independent of the radial position. This assumption is justified by the fact that the contact area is very small ($b \ll 0.1\text{mm}$ for $F < 100\text{N}$, cf. equation (4) below).

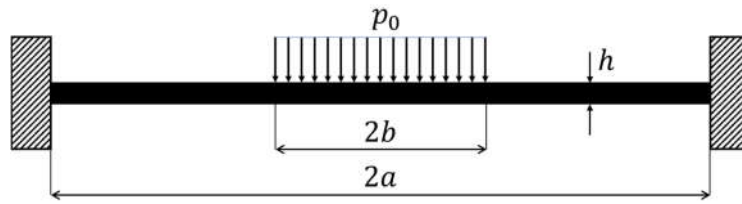


Figure 3: parameters of a circular plate model, figure not to scale

The contact radius b is obtained by Hertzian contact theory [28]:

135

$$b = \left(\frac{3 \cdot F \cdot r}{4 \cdot E^*} \right)^{1/3} \quad \frac{1}{E^*} = \frac{1 - \nu^2}{E} + \frac{1 - \nu_p^2}{E_p} = \frac{1}{E'} + \frac{1}{E'_p} \quad (4)$$

with E , ν , E_p , ν_p being the elasticity modulus and Poisson ratio of the SP specimen and of the puncher respectively. The indentation depth of the puncher into the SP specimen (without plate bending deflection) is:

136

137

138

$$y_{\text{ind}} = \frac{b^2}{r} = \left[\frac{3F}{4E^*} \right]^{2/3} \cdot r^{-1/3} \quad (5)$$

According to Reissner's plate theory, the linear-elastic solution for the central deflection of a fully clamped circular plate is given by [29–31]:

139

140

$$u_0 = \frac{F a^2}{64 \pi N} \left[4 - \left(\frac{b}{a} \right)^2 \left(3 - 4 \ln \left(\frac{b}{a} \right) \right) + \frac{16}{5(1 - \nu)} \cdot \left(\frac{h}{a} \right)^2 \cdot \left(1 - 2 \ln \left(\frac{b}{a} \right) \right) \right] \quad (6)$$

$$F = p_0 \pi b^2 \quad N = \frac{E h^3}{12(1 - \nu^2)}$$

where h is the plate thickness and p_0 the contact pressure. The rightmost term accounts for the shear deformation of the plate. Despite of the consideration of the shear rotation of the cross section, equation (6) relies on the assumption of thin plates, i.e. $h \ll a$. Comparing FE calculations with equation (6), it was found that the elastic slope is underestimated for higher thicknesses of the plate (see Figure 4).

141

142

143

144

145

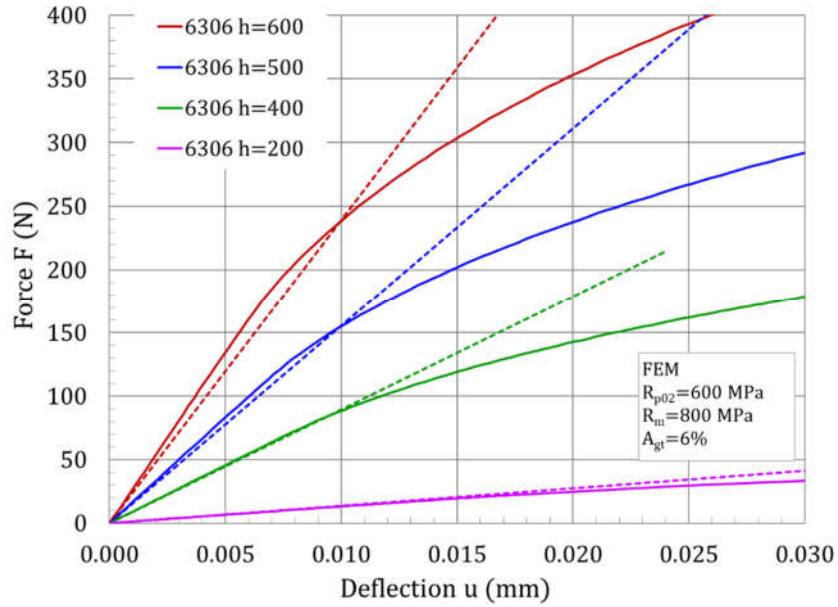


Figure 4. Comparison of the $F(u)$ slope according to equation (6) (dashed lines) with FEM simulations for different sample thicknesses (200, 400, 500, 600 μm). 146
147
148

It was concluded that the h/a dependence of shear term in equation (6) has to be modified. A systematic variation of the shear term and comparison with elastic FE solutions for different plate thicknesses was performed. A very good approximation is obtained by the following equation (see also Figure 5): 149
150
151
152

$$u_0 = \frac{F a^2}{64\pi N} \left[4 - \left(\frac{b}{a}\right)^2 \left(3 - 4 \ln\left(\frac{b}{a}\right) \right) + \frac{1.0565}{(1-\nu)} \cdot \left(\frac{h}{a}\right)^{4/3} \cdot \left(1 - 2 \ln\left(\frac{b}{a}\right) \right) \right] \quad (7)$$

The modified elastic slope is defined as: 153

$$S_{el} = \frac{F}{u} = \frac{64\pi N}{a^2 \cdot f(b/a)} \quad (8)$$

$$f\left(\frac{b}{a}\right) = \left[4 - \left(\frac{b}{a}\right)^2 \left(3 - 4 \ln\left(\frac{b}{a}\right) \right) + \frac{1.0565}{(1-\nu)} \cdot \left(\frac{h}{a}\right)^{4/3} \cdot \left(1 - 2 \ln\left(\frac{b}{a}\right) \right) \right]$$

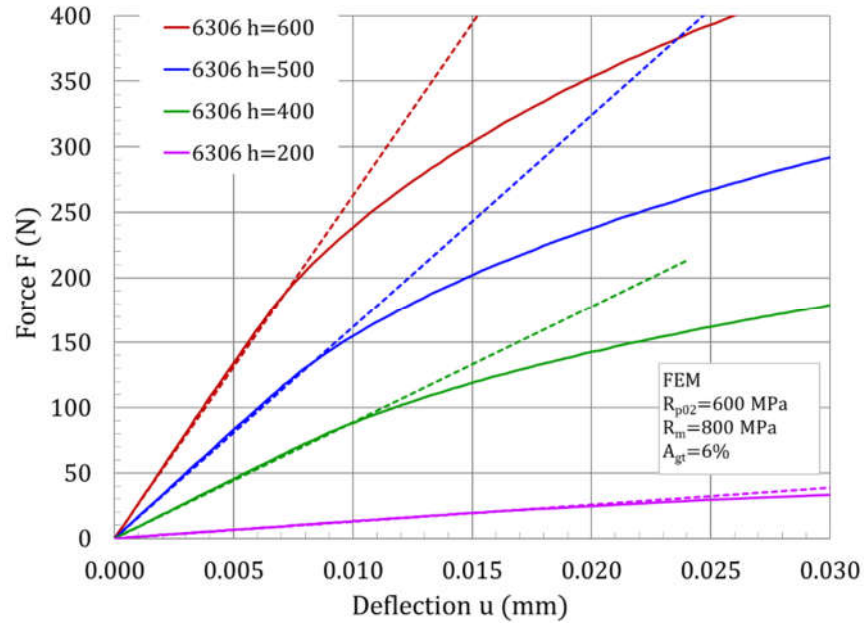


Figure 5. Comparison of the $F(u)$ slope according to equation (7) with FEM simulations for different sample thicknesses (200, 400, 500, 600 μm).

The reference force for the elastic slope is chosen based on the plate stiffness as follows:

$$F \cdot \frac{a^2}{N} = u_{0,\text{ref}} = 0.01 \cdot a \rightarrow F_{\text{ref}} = 0.01 \cdot \frac{N}{a} \rightarrow F_{\text{ref}} \propto h^3/a \quad (9)$$

The combination of equations (9) and (4) gives:

$$b(F_{\text{ref}}) = b_{\text{ref}} = \left[\frac{E' \cdot h^3 \cdot r}{1600 \cdot E^* \cdot a} \right]^{1/3} \quad (10)$$

For the standard geometry with the parameters $F_{\text{ref}} = 10.4 \text{ N}$, $a = 2.2 \text{ mm}$, $E = 200 \text{ GPa}$, $E_p = 565 \text{ GPa}$, $\nu = \nu_p = 0.3$, $r = 1.25 \text{ mm}$, and $h = 0.5 \text{ mm}$, one obtains the initial slope of the $F(u)$ curve as $S_{\text{el}} = 16.1 \text{ kN/mm}$. It has to be mentioned, that the calculation of the contact radius and indentation depth by equations (4) and (5) is a rigorous simplification. In contrast to this elastic approach, there is an immediate plastic deformation at the upper surface of the sample in the contact region, section 3. Nevertheless, the deflection of the plate according to equation (7) is rather insensitive to the contact radius b as long as $b \ll a$ holds. Therefore, the analytical calculation of the elastic slope works surprisingly well.

2.3. Systematic variation of the tensile parameters and specimen thickness

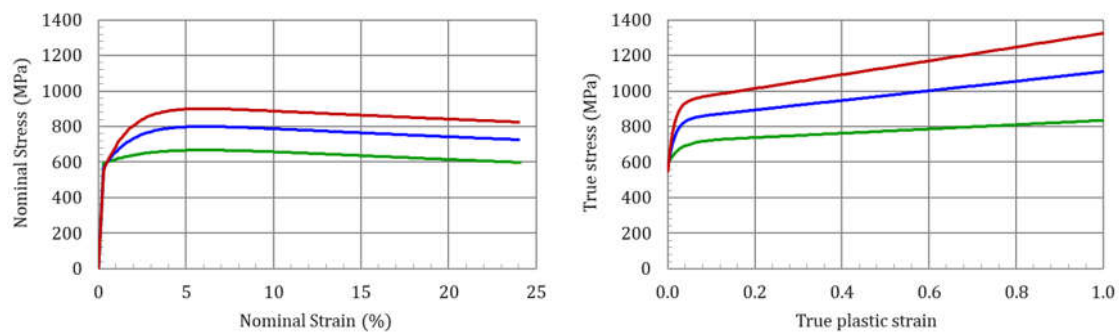
A generic material behavior was used for the FE simulations. Three levels of YS (300, 600 and 900 MPa) and for each YS three different yield ratios were applied to generate the stress-strain curves according to equations (2) and (3). The uniform elongation was varied for the medium yield stress and yield ratio by $A_{\text{gt}} = 3, 6$ and 12% and was kept constant at 6% otherwise. The range of these material properties is typical for various classes of steel. An iterative fitting algorithm was used to obtain the constitutive parameters σ_{y0} , r_1 and n as used in equation (2), section 2.1, for a given set of R_{p02} , R_m and A_{gt} . The parameter variations are listed in Table 2. The nominal and true stress-strain curves for selected parameter combinations are shown in Figure 6.

Table 2. Material parameters for the investigation of the yield strength correlation, see equation (2).

Code	S_{y0} (MPa)	r_1 (MPa)	n	R_{p02} (MPa)	R_m (MPa)	R_m/R_{p02}	A_{gt} (%)
3106	296.3	60.8	35.4	300	333	1.11	6
3306	285.3	135.1	59.2	300	400	1.33	6
3506	275.2	193.9	69.1	300	450	1.5	6
6106	592.2	121.2	27.5	600	667	1.11	6
6303	504.2	311.3	185.9	600	800	1.33	3
6306	569.0	270.0	62.6	600	800	1.33	6
6312	587.7	298.6	22.1	600	800	1.33	12
6506	547.5	388.8	73.4	600	900	1.5	6
9106	887.9	179.2	39.4	900	1000	1.11	6
9306	851.0	404.9	66.2	900	1200	1.33	6
9506	816.3	585.3	78.3	900	1350	1.5	6

180
181

182

**Figure 6.** Generic stress-strain curves for $R_{p02}=600$ MPa and varying R_m/R_{p02} , codes 6106 (green), 6306 (blue), 6506 (red); left: nominal stress vs. total nominal strain; right: true stress vs. true plastic strain.183
184
185

In addition, FE simulations are executed with different thicknesses of the SP disc, in particular $h = 200, 400, 500, 600$ μm . In order to discriminate the multitude of simulations, a simulation-ID is defined as follows: $xxxx-hy$, where $xxxx$ stands for the material code (see Table 2) and y for the thickness (2 for $h = 200$ μm etc). For example, 6306-h4 refers to parameter set $R_{p02} = 600$ MPa, $R_m = 800$ MPa, $A_{gt} = 6\%$, $h = 400$ μm . In total, 20 simulations were carried out, see Table 3 in section 3.

186
187
188
189
190
191

3. Results

192

Selected force-deflection curves for the chamfer geometry are shown in Figure 7. Both yield strength variation at constant yield ratio and variation of yield ratio at constant yield strength produce significant effects in the curves. While in the first case an effect can be observed right at the onset of plastic deformation, the curves start to deviate somewhat later in the latter case. In the right figure, the range of transition forces F_e (obtained by the currently used bi-linear fit, see Figure 1) is indicated. From this it becomes clear, that the plastic deformation in the sample is already well advanced when the deflection u_A is reached.

193
194
195
196
197
198
199
200

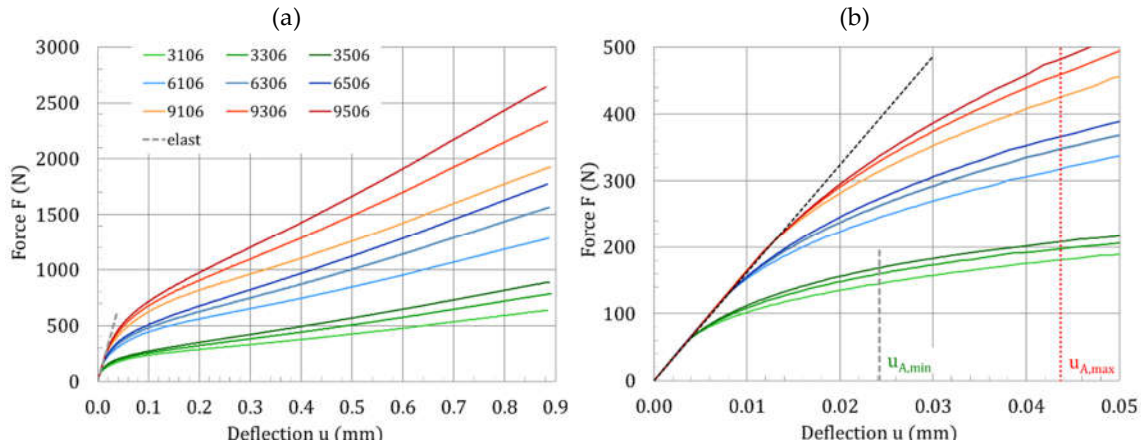


Figure 7. Force-deflection curves for different flow parameters (material codes xx06 from Table 2, $h = 500 \mu\text{m}$); left (a): complete curves; right (b): zoom into the lower deflection range with indication of the elastic slope and the range where the transition forces F_e from the bi-linear fits are located.

These results straightforwardly suggest a modified definition of the elastic-plastic transition force. A disjunctive combination of the horizontal and the vertical distance of $F(u)$ from the elastic slope is proposed:

$$u(F) > \frac{F}{S_{el}} + \frac{a}{1100} \vee F(u) < S_{el} \cdot \left(u - \frac{a}{2200}\right) \quad (11)$$

with S_{el} being the elastic slope as defined in equation (8). The first fulfilment of equation (11), whichever criterion is reached earlier, marks the modified transition force F_y . An example of this procedure is shown in Figure 8.

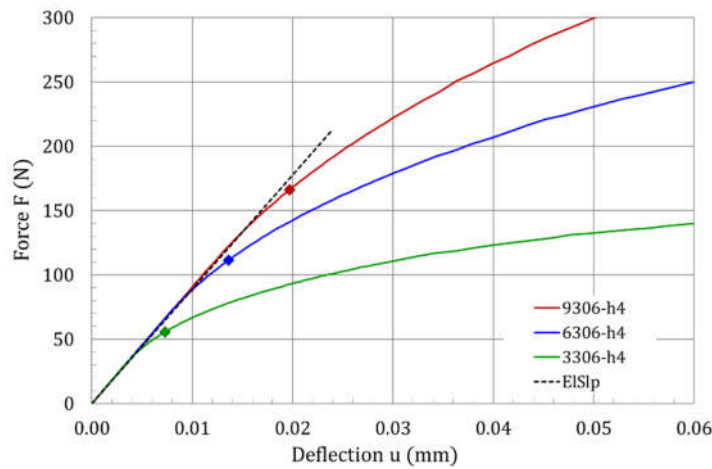


Figure 8. Force-deflection curves for simulation-IDs x306-h4 with transition forces F_y marked by diamonds.

It should be mentioned that the agreement of the analytical elastic slope and the very first stage of the FE solution is only existing for the force-deflection curve $F(u)$, not for the force-displacement curve $F(v)$. This is due to the indentation process between punch and upper specimen surface, which takes place immediately after the contact, see Figure 9. Therefore, the proposed transition force F_y can only be determined from $F(u)$ measurements, not from $F(v)$.

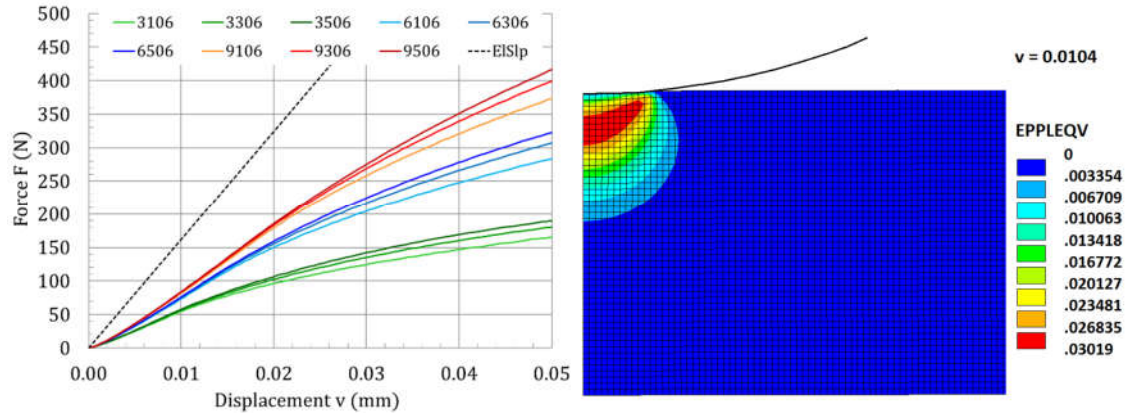


Figure 9. Force-displacement curves $F(v)$ and elastic slope with parameters as in Figure 7 (left); plastic equivalent strain distribution at $v = 0.0104$ mm for simulation-ID 6306-h5 (right).

219
220

The summary of all simulation results is listed in Table 3. Both methods for the evaluation are included (F_e based on bi-linear fitting [6] vs. F_y based on equations (4), (5) and (8)–(11)).

221
222
223

Table 3. Transition forces and obtained correlation factors.

224

Simulation-ID	F_y (N)	F_e (N)	$\beta_{YS}(F_y)$	$\beta_{YS}(F_e)$
3106-h5	81.9	196.4	0.916	0.382
3306-h2	13.3	24.8	0.900	0.484
3306-h4	55.8	124.7	0.860	0.385
3306-h5	85.5	202.5	0.877	0.370
3306-h6	120.1	301.0	0.899	0.359
3506-h5	88.5	209.6	0.848	0.358
6106-h5	164.2	370.6	0.914	0.405
6303-h5	178.8	401.8	0.839	0.373
6306-h2	25.9	42.3	0.927	0.567
6306-h4	111.4	232.7	0.862	0.413
6306-h5	174.7	392.8	0.859	0.382
6306-h6	244.5	586.7	0.884	0.368
6312-h5	167.4	381.1	0.896	0.394
6506-h5	179.5	407.1	0.836	0.368
9106-h5	250.6	539.6	0.898	0.417
9306-h2	38.5	55.4	0.935	0.650
9306-h4	168.4	335.8	0.855	0.429
9306-h5	264.0	563.3	0.852	0.399
9306-h6	369.2	850.2	0.878	0.381
9506-h5	269.9	578.5	0.834	0.389

The resulting correlation factors for the yield strength are obtained from (see also equation (1)):

225
226

$$\beta_{YS}(F_e, F_y) = \frac{R_{p02} \cdot h^2}{(F_e, F_y)} \quad (12)$$

4. Discussion

227

The modified transition force F_y is essentially different from the one obtained from bilinear fitting, F_e (see section 1). As shown in Figure 10, F_y is associated to a significantly earlier stage of the SP test as compared to F_e . Therefore, it can be expected that F_y is mainly

228
229
230

governed by the onset of plastic flow. In contrast, F_e is significantly affected by the work hardening of the material and thus less representative for the onset of plastic flow.

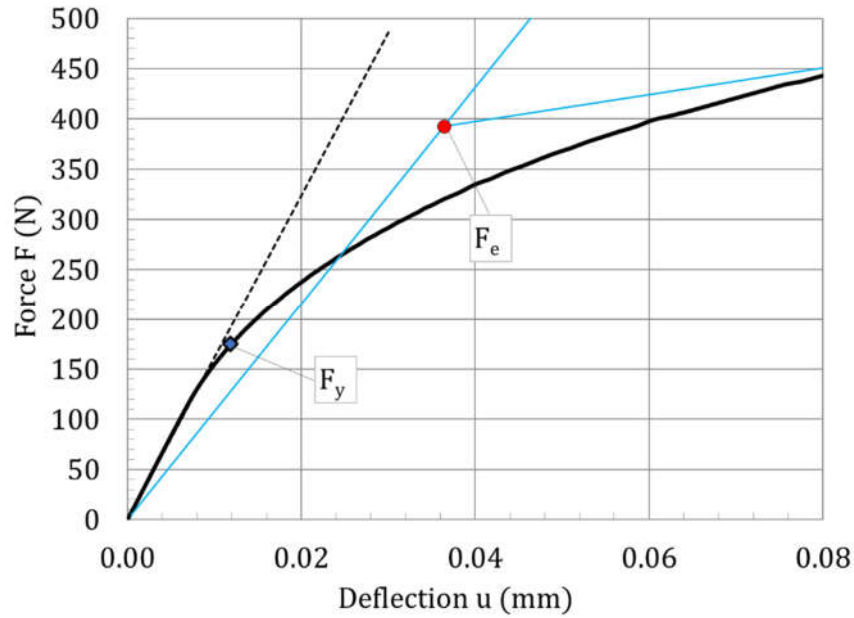


Figure 10. Force-deflection curve with transition forces F_y (according to section 3 and F_e from bi-linear fitting); simulation-ID 6306-h5.

This reasoning is underpinned by the plastic strain fields associated with F_y and F_e respectively. The equivalent plastic strain is shown in Figure 11.

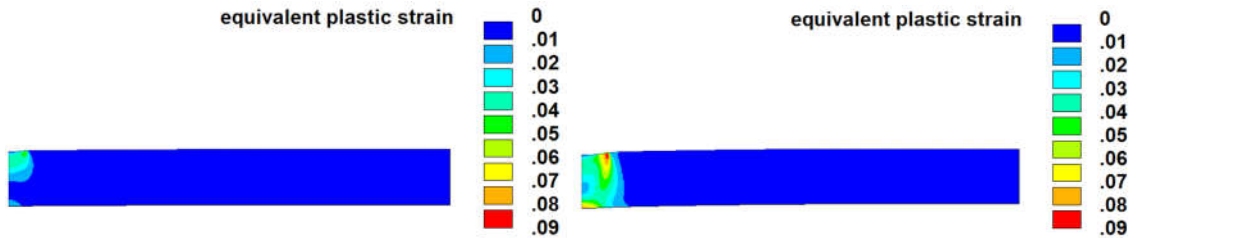


Figure 11. Equivalent plastic strain fields in the sample associated with F_y (left) and F_e (right), Sim-ID 6306-h5, same scale in both plots.

In Table 4, the simulation results, as listed in Table 3, are analyzed from a statistical point of view. Various data sets are selected and for each selection the average correlation factors $\bar{\beta}_{YS}$ are listed along with their coefficients of variation c_V (standard deviation divided by mean value).

Table 4. Average correlation factors and coefficients of variation (standard deviation divided by average).

Data set	$\bar{\beta}_{YS}(F_e)$	$\bar{\beta}_{YS}(F_y)$	$c_V(F_e)$	$c_V(F_y)$
All data	0.41	0.88	17.4%	3.7%
Sets $h = 600 \mu\text{m}$	0.37	0.88	2.5%	1.9%
Sets $h = 500 \mu\text{m}$	0.39	0.87	4.4%	3.8%
Sets $h = 400 \mu\text{m}$	0.41	0.86	4.4%	0.3%
Sets $h = 200 \mu\text{m}$	0.57	0.92	12.0%	1.1%

From these data it is obvious that the scatter of the correlation factor values obtained by the F_e approach is significantly larger as compared to the new F_y approach. Therefore, it can be expected that the estimation of the yield strength based on F_y is more precise. Moreover, the F_e based correlation factor exhibits a significant dependence on the sample thickness. This effect is much less pronounced in the F_y based correlation factor. This is understandable, as the estimation of the elastic slope S_{el} (section 2.2) explicitly considers the sample geometry, in particular the sample thickness in relation to the plate diameter (h/a) and the punch radius r . In conclusion, $\beta_{YS}(F_e)$ is to a much larger extent dependent on the geometry and the flow properties of the material. On the other hand, the $\beta_{YS}(F_y)$ correlation factor can be used for different geometrical set-ups, e. g. the so-called TEM geometry ($r = 0.5$ mm, $D = 1.75$ mm, $h = 250$ μ m) which is also mentioned in [6]. For this geometry and material code 6306, one obtains the following transition forces and correlation factors:

Sim-ID	F_y (N)	F_e (N)	$\beta_{YS}(F_y)$	$\beta_{YS}(F_e)$
6306-D175-h250	42.7	95.5	0.88	0.39

The correlation coefficient $\beta_{YS}(F_y)$ agrees well with the one obtained for the standard geometry.

5. Conclusions

The effect of flow properties and SP geometry on the lower range of the force-deflection curve $F(u)$ was analyzed by a systematic finite element study. Reissner's plate theory was employed to develop an analytical set of equations for the elastic slope of the force-deflection curve. A correction of the shear term was proposed. The results can be summarized as follows:

- The analytical elastic slope agrees very well with the finite element simulation.
- A modified elastic-plastic transition force F_y was proposed for the empirical yield strength correlation, which provides a significantly reduced uncertainty as compared to the elastic-plastic transition force F_e defined in the European standard.
- With the new definition of F_y (equation 11), the yield strength correlation is widely independent of the SP geometry and the flow properties of the material.

The presented work provides an improvement for the estimation of the yield strength from force-deflection curves of small punch tests through a significant reduction of uncertainties and a better independence of the small punch geometry. At the same time the procedure is kept as simple as possible for practical application. The new definition of the elastic-plastic transition force can be considered in future revisions of the related standard EN-10371.

Acknowledgments: The work contributes to the Joint Programme on Nuclear Materials (JPNM) within the European Energy Research Alliance (EERA). The work is also an in-kind contribution to the H2020-Euratom project FRACTESUS (grant agreement no. 900014).

Data Availability: The raw/processed data required to reproduce these findings cannot be shared at this time as the data also forms part of an ongoing study.

List of abbreviations

a	Effective lower die radius	288
A_{gt}	Total uniform strain (nominal strain at $\bar{\sigma} = R_m$)	289
b	Radius of the contact area between punch and specimen	290
b_{ref}	Contact radius associated with the reference force	291
c_V	Coefficient of variation (standard deviation divided by average)	292
D	Diameter of lower die receiving hole	293

E	Elasticity modulus	295
F	Punch force	296
F_e	Elastic-plastic transition force	297
F_{ref}	Reference force for the analytical calculation of the elastic slope	298
F_y	Modified elastic-plastic transition force	299
FE	Finite element	300
h	Specimens thickness	301
n	Hardening exponent of the true stress-plastic strain curve	302
N	Plate stiffness	303
r	Puncher radius	304
R^2	Coefficient of determination	305
r_1	Parameter of the true stress-plastic strain curve	306
$R_{p0.2}$	Yield strength	307
R_m	Ultimate tensile strength	308
S_{el}	Elastic slope of the small punch plate (analytical calculation)	309
SP	Small punch	310
UTS	Ultimate tensile strength	311
u	Central deflection at the specimen bottom (opposite to punch tip)	312
v	Punch tip displacement	313
y_{ind}	Indentation depth of the punch as calculated by Hertzian contact theory	314
YS	Yield strength	315
β_{YS}	Empirical factor for the estimation of yield stress	316
ε	True strain	317
$\bar{\varepsilon}$	Nominal strain	318
ν	Poisson's ratio	319
σ	True stress	320
$\bar{\sigma}$	Nominal stress	321
σ_{Y0}	Elasticity limit, true initial flow stress	322

References

- | | | |
|------|--|-------------------|
| [1] | J. Kameda, A kinetic model for ductile-brittle fracture mode transition behavior, <i>Acta Metall.</i> 34 (1986) 2391–2398. https://doi.org/10.1016/0001-6160(86)90142-2 . | 324
325 |
| [2] | T. Misawa, T. Adachi, M. Saito, Y. Hamaguchi, Small punch tests for evaluating ductile-brittle transition behavior of irradiated ferritic steels, <i>J. Nucl. Mater.</i> 150 (1987) 194–202. https://doi.org/10.1016/0022-3115(87)90075-4 . | 326
327 |
| [3] | M. Abendroth, M. Kuna, Identification of ductile damage and fracture parameters from the small punch test using neural networks, <i>Eng. Fract. Mech.</i> 73 (2006) 710–725. https://doi.org/10.1016/j.engfracmech.2005.10.007 . | 328
329 |
| [4] | T. Melkior, D. Terentyev, C. Chang, A. Bakaev, S. Holmström, S. Lebediev, A. Paputsia, Mechanical properties of structural metallic alloys for nuclear applications deduced by small punch test, <i>J. Nucl. Mater.</i> 583 (2023) 154521. https://doi.org/10.1016/j.jnucmat.2023.154521 . | 330
331
332 |
| [5] | Y. Shen, S. Lv, Q. Zhou, L. Shi, L. Sun, Z. Li, Microstructure Characterization and Small Punch Test Analysis in Nickel-Based Alloy 617 by High Energy Neon Implantation, <i>Metals.</i> 12 (2022) 438. https://doi.org/10.3390/met12030438 . | 333
334 |
| [6] | EN Standard EN-10371, Small punch test method for metallic materials, 2021. | 335 |
| [7] | E. Altstadt, F. Bergner, M. Houska, Use of the small punch test for the estimation of ductile-to-brittle transition temperature shift of irradiated steels, <i>Nucl. Mater. Energy.</i> 26 (2021) 100918. https://doi.org/10.1016/j.nme.2021.100918 . | 336
337 |
| [8] | J. Calaf Chica, P. Bravo Díez, M. Preciado Calzada, A New Prediction Method for the Ultimate Tensile Strength of Steel Alloys with Small Punch Test, <i>Materials.</i> 11 (2018) 1491. https://doi.org/10.3390/ma11091491 . | 338
339 |
| [9] | J. Calaf Chica, P.M. Bravo Díez, M. Preciado Calzada, Development of an improved prediction method for the yield strength of steel alloys in the Small Punch Test, <i>Mater. Des.</i> 148 (2018) 153–166. https://doi.org/10.1016/j.matdes.2018.03.064 . | 340
341 |
| [10] | S. Holmström, I. Simonovski, D. Baraldi, M. Bruchhausen, E. Altstadt, R. Delville, Developments in the estimation of tensile strength by small punch testing, <i>Theor. Appl. Fract. Mech.</i> 101 (2019) 25–34. https://doi.org/10.1016/j.tafmec.2019.01.020 . | 342
343 |
| [11] | E. Altstadt, M. Houska, I. Simonovski, M. Bruchhausen, S. Holmström, R. Lacalle, On the estimation of ultimate tensile stress from small punch testing, <i>Int. J. Mech. Sci.</i> 136 (2018) 85–93. https://doi.org/10.1016/j.ijmecsci.2017.12.016 . | 344
345 |

- [12] E.N. Campitelli, P. Spätig, R. Bonadé, W. Höffelner, M. Victoria, Assessment of the constitutive properties from small ball punch test: experiment and modeling, *J. Nucl. Mater.* 335 (2004) 366–378. <https://doi.org/10.1016/j.jnucmat.2004.07.052>. 346
347
- [13] R. Lacalle, D. Andrés, J.A. Álvarez, F. Gutiérrez-Solana, Transition Region of Nuclear Vessel Steels: Master Curve Approach Using Small Punch Notched Specimens, *Key Eng. Mater.* 734 (2017) 77–86. 348
<https://doi.org/10.4028/www.scientific.net/KEM.734.77>. 349
350
- [14] D. Andres, R. Lacalle, S. Cicero, J.A. Alvarez, Application of the small punch test in combination with the master curve approach for the characterisation of the ductile to brittle transition region, *J. Nucl. Mater.* 518 (2019) 409–418. 351
<https://doi.org/10.1016/j.jnucmat.2019.03.011>. 352
353
- [15] S. Holmström, Y. Li, P. Dymacek, E. Vacchieri, S.P. Jeffs, R.J. Lancaster, D. Omacht, Z. Kubon, E. Anelli, J. Rantala, A. Tonti, S. Komazaki, Naveena, M. Bruchhausen, R.C. Hurst, P. Hähner, M. Richardson, D. Andres, Creep strength and minimum strain rate estimation from Small Punch Creep tests, *Mater. Sci. Eng. A.* 731 (2018) 161–172. <https://doi.org/10.1016/j.msea.2018.06.005>. 354
355
356
- [16] P. Dymáček, M. Jarý, F. Dobeš, L. Kloc, Tensile and Creep Testing of Sanicro 25 Using Miniature Specimens, *Materials*. 11 (2018) 142. <https://doi.org/10.3390/ma11010142>. 357
358
- [17] J. Vivas, C. Capdevila, E. Altstadt, M. Houska, I. Sabirov, D. San-Martín, Microstructural Degradation and Creep Fracture Behavior of Conventionally and Thermomechanically Treated 9% Chromium Heat Resistant Steel, *Met. Mater. Int.* (2018). <https://doi.org/10.1007/s12540-018-0192-6>. 359
360
361
- [18] J. Peng, M. Gao, H. Zhang, X. Geng, X. Liu, H. Pan, Small punch creep test reveals the differences of high-temperature creep behaviours for laser powder bed fusion and Rolled Inconel 718 alloys, *Mater. Sci. Eng. A.* 886 (2023) 145698. 362
<https://doi.org/10.1016/j.msea.2023.145698>. 363
364
- [19] Y. Huang, M. Kadowaki, T. Nakano, K. Kumada, S. Watanabe, T. Kawada, K. Sato, Creep constitutive law prediction via short-term evaluation using a small size testing method, *Energy Rep.* 10 (2023) 1126–1134. <https://doi.org/10.1016/j.egy.2023.07.046>. 365
366
- [20] Š. Hermanová, Z. Kuboň, P. Čížek, J. Kosňovská, G. Rožnovská, O. Dorazil, M. Cieslarová, Study of Material Properties and Creep Behavior of a Large Block of AISI 316L Steel Produced by SLM Technology, *Metals*. 12 (2022) 1283. 367
<https://doi.org/10.3390/met12081283>. 368
369
- [21] X. Tian, S. Zhang, H. Xu, T. Li, B. Yang, M. Zhang, Assessment of Creep Properties Using Small Punch Test for a 9%Cr-Mo-Co-B Power Plant Steel, *Metals*. 11 (2021) 1996. <https://doi.org/10.3390/met11121996>. 370
371
- [22] H. Pan, J. Peng, X. Geng, M. Gao, X. Miao, Prediction of mechanical properties for typical pressure vessel steels by small punch test combined with machine learning, *Int. J. Press. Vessels Pip.* 206 (2023) 105060. <https://doi.org/10.1016/j.ijpvp.2023.105060>. 372
373
- [23] J. Zhong, Z. He, K. Guan, T. Jiang, Investigation on regression model for the force of small punch test using machine learning, *Int. J. Press. Vessels Pip.* 206 (2023) 105031. <https://doi.org/10.1016/j.ijpvp.2023.105031>. 374
375
- [24] J. Kameda, X. Mao, Small-punch and TEM-disc testing techniques and their application to characterization of radiation damage, *J. Mater. Sci.* 27 (1992) 983–989. <https://doi.org/10.1007/BF01197651>. 376
377
- [25] E. Altstadt, H.E. Ge, V. Kuksenko, M. Serrano, M. Houska, M. Lasan, M. Bruchhausen, J.-M. Lapetite, Y. Dai, Critical evaluation of the small punch test as a screening procedure for mechanical properties, *J. Nucl. Mater.* 472 (2016) 186–195. 378
<https://doi.org/10.1016/j.jnucmat.2015.07.029>. 379
380
- [26] P. Hähner, C. Soyarslan, B. Gülçimen Çakan, S. Bargmann, Determining tensile yield stresses from Small Punch tests: A numerical-based scheme, *Mater. Des.* 182 (2019) 107974. <https://doi.org/10.1016/j.matdes.2019.107974>. 381
382
- [27] J. Zhong, M. Song, K. Guan, P. Dymacek, Application of a database in the evaluation of strengths of Cr-Mo steels by means of small punch test, *Int. J. Mech. Sci.* 166 (2020) 105195. <https://doi.org/10.1016/j.ijmecsci.2019.105195>. 383
384
- [28] V.L. Popov, Contact mechanics and friction: physical principles and applications, English ed., Springer, Heidelberg ; New York, 2010. 385
386
- [29] F.U. Mathiak, Ebene Flächentragwerke II - Grundlagen der Plattentheorie, (2008). 387
- [30] E. Reissner, On the Theory of Bending of Elastic Plates, *J. Math. Phys.* 23 (1944) 184–191. 388
<https://doi.org/10.1002/sapm1944231184>. 389
- [31] R.D. Mindlin, Influence of Rotatory Inertia and Shear on Flexural Motions of Isotropic, Elastic Plates, *J. Appl. Mech.* 18 (1951) 31–38. 390
391
392

Disclaimer/Publisher's Note: The statements, opinions and data contained in all publications are solely those of the individual author(s) and contributor(s) and not of MDPI and/or the editor(s). MDPI and/or the editor(s) disclaim responsibility for any injury to people or property resulting from any ideas, methods, instructions or products referred to in the content. 393
394
395